Visible light optical coherence tomography measures retinal oxygen metabolic response to systemic oxygenation

Ji Yi, Wenzhong Liu, Siyu Chen, Vadim Backman, Nader Sheibani, Christine M. Sorenson, Amani A. Fawzi, Robert A. Linsenmeier, and Hao F. Zhang

Table of content

Supplementary methods for oxygen metabolic rate quantification and microvasculature visualization

Vis-OCT system and data acquisition. Vis-OCT used a supercontinuum source as illumination. The wavelength range that we collected was from 500 nm to 620 nm. An open-space Michelson interferometry configuration was adopted in the vis-OCT system due to its minimum optical dispersion. The beam was collimated and split by a cube beam splitter (Supplementary Fig. S1) into the reference and sample arms. The sample arm contained a two-dimensional galvanometer mirror to steer the beam, and a 0.2 magnification Keplerian telescope to relay the beam from the galvanometer mirror to the rat's pupil plane. The reference arm consisted of a few dispersion control glass plates, and a mirror to reflect the beam. The two beams from the reference and sample arms recombined at the beam splitter and were collected by an optical fiber. The fiber delivered the light to a home-made spectrometer, which consisted of a collimating lens, a diffraction grating, an objective lens, and a line scan CCD camera (Balser, sprint slp2k). The camera exposure and the scanning galvo mirror were synchronized by an analog output card (PCI6731, National Instrument). Two protocols were used in our experiment. Protocol 1 scanned a 7.8 mm^2 transverse plane on the retina at an A-line rate of 25 kHz. Each B-scan had 256 A-scans and the protocol had a total of 256 B-scans. Protocol 2 scanned two concentric circles centered at optic disk with 4096 pixels in each circle, at an A-line rate of 70 kHz. The dual circle scan pattern then was repeated 8 times. The total A-line number in both protocols was 65,536. We used a three-lead EKG system to collect the EKG signals. The EKG signal collection was also synchronized with the scanning by the analog output card, so that the collections of EKG and the OCT image were simultaneous.

Vis-OCT signal processing and quantification. Each exposure of the CCD camera recorded an interferometric spectrum. We first removed the DC spectral background averaged from the entire 65,536 spectral signals, and resampled the remaining spectrum into *k*-space with an equal interval. The complex reflectance signal with respect to depth (A-line or A-scan) was obtained by a fast Fourier transform (FFT) on the k-space spectrum. The process was repeated for all 65,536 A-lines and the 3D complex reflectance data was produced. By taking the amplitude of the complex reflectance, we obtained the 3D morphological image. Supplementary Fig. S2 shows the flow chart for the step by step data processing methods used to calculate $rMRO_2$.

Hemoglobin oxygen saturation (sO_2) quantification. We derived sO_2 values from the scanning protocol 1. The processing involved the following three steps: 3D image blood vessel segmentation, spectral extraction, and fitting.

1) 3D image vessel segmentation. Because the largest retinal blood vessels run on the

surface of the retina, we first detected the surface of the retina by intensity thresholding. An intensity histogram adjustment was performed on each B-scan image to maximize contrast. Next, a global image threshold calculated using Otsu's methods was used to binarize the image [1]. Then the depth location of the first non-zero boundary from each A-scan was recorded as the surface at that point. The same procedure was repeated on all the 256 B-scans.

We then located the transverse coordinates of the blood vessels. A mean intensity projection from a slab around 150 to 200μm deep from the surface was taken. An adaptive thresholding procedure was taken to binarize the image. In order to remove the noise, we performed an image dilation and erosion processing on the binarized image with a 3 pixel-radian disk pattern. Each vessel then could be separated and selected individually. The 3D coordinates (axial and transverse) were then recorded to further extract the spectrum from blood vessels.

2) **Spectra extraction and fitting.** Given the 3D coordinates of each blood vessel, the corresponding interferometric spectra were selected from the raw data and Short-time Fourier transform (STFT) were performed. A Gaussian window size k_w = 0.32 μm^{-1} (17-nm bandwidth at 585-nm center wavelength) was used in the STFT, reducing the axial resolution to 9 μm. The spectra were then taken from the bottom blood vessel wall. The spectral fitting model and the methods have been described in Ref. [2]. Briefly, the OCT signal can be modeled as

$$I^2(\lambda) = I_0^2(\lambda) R_0 r(\lambda) \exp[-2d\mu_{HbO2}(\lambda) \times sO_2 - 2d\mu_{Hb}(\lambda) \times (1 - sO_2)], \quad (1)$$

where $I_0(\lambda)$ is the incident intensity on the retina. We ignored the optical attenuation by ocular lens and vitreous chamber and, thus, took the source spectrum as I_0; R_0 is the reference arm reflectance; d [mm] is the vessel diameter; $r(\lambda)$ [dimensionless] is the reflectance at the vessel wall, whose scattering spectrum can be modeled as a power law under the first-order Born approximation $r(\lambda) = A\lambda^{-\alpha}$, where A is a constant. The optical attenuation coefficient μ [mm^{-1}] combines the absorption (μ_a) and scattering coefficients (μ_s) of whole blood, which are both wavelength- and oxygenation- dependent. The subscripts Hb and HbO_2 denote the contribution from deoxygenated and oxygenated blood, respectively. A linear regression to the spectra returned the value of sO_2.

Blood flow quantification. We derived blood flow from the scanning protocol 2. The principle has been described in previous publications [3, 4]. We employed the phase sensitive Doppler OCT for blood flow measurement. In phase sensitive Doppler-OCT, signals from two adjacent A-lines (Supplementary Fig. S3a) were used to extract the velocity of optical scatterers. The blood flow velocity can be expressed as

$$v = \frac{f_{\text{sample}} \cdot \lambda_0 \cdot \Delta\phi}{4 \cdot \pi \cdot n \cdot \cos(\theta)} \tag{2}$$

where f_{sample} is the OCT A-line scanning frequency; λ_0 [nm] is the center wavelength of the light source; $\Delta\phi$ is the phase shift of the complex reflectance between adjacent A-scans [radians]; n is the refraction index of the sample; and θ [radians] is the Doppler angle; the angle between the blood vessel and probing light (Supplementary Fig. S3b). The velocity projected to the probe beam direction v_p is proportional to $\Delta\phi$,

$$v_p = \frac{f_{sample} \cdot \lambda_0 \cdot \Delta\phi}{4\pi n} \tag{3}$$

The total blood flow is equal to the product of the velocity and the vessel cross section

$$F = v \times A = v \times \frac{\pi Dia^2}{4} \times \sin(\theta) = v_p \times \frac{\pi Dia^2}{4} \times \tan(\theta) \tag{4}$$

Thus, the post-processing for blood flow included the following steps: calculation of the projected blood velocity v_p, Doppler angle θ, and blood vessel diameter Dia.

1) **Projected velocity calculation.** We first obtained the complex reflectance A-line signal from the Fourier transform of the interferometric spectra. Next, we took the derivative of the phase term of the complex signal between the adjacent A-lines. Then a 5 by 5 median filter was applied to the B-scan phase image to remove the salt and pepper noise (Supplementary Fig. S3d). $\Delta\phi$ is calculated by the integration of the phase shift within each vessel lumen. The other systematic parameters are: f_{sample} = 70 kHz; λ_0 = 568nm; and n=1.38. The v_p then was calculated by Eq. 3.
2) **Doppler angle calculation.** According to the Supplementary Fig. S3b, dual circle scans with radius r_1 and r_2 intersect a vessel at two different vessel center points, $S(x_1,y_1,z_1)$ and $E(x_2,y_2,z_2)$. The direction of the vessel can be expressed as a vector $\overrightarrow{ES}$

$$\overrightarrow{ES} = (x_1 - x_2, y_1 - y_2, z_1 - z_2) \tag{5}$$

The direction of probing light is $\overrightarrow{NS'}$, where N is the nodal point of the eye. If the eye diameter is h, then the coordinates of N are $(0,0,h)$ and the coordinates of S' are $(x_1',y_1',0)$. The probing light direction $\overrightarrow{NS'}$ is:

$$\overrightarrow{NS'} = (x_1', y_1', -h) \tag{6}$$

The Doppler angle θ can then be calculated given the coordinates of all the vectors:

$$\cos(\theta) = \frac{\overrightarrow{ES} \cdot \overrightarrow{NS'}}{|\overrightarrow{ES}| \cdot |\overrightarrow{NS'}|} \tag{7}$$

The (x,y) coordinates of E and S are obtained by

$$\begin{aligned} x_1 &= r_1 \times \cos(\varphi_1) \\ x_2 &= r_2 \times \cos(\varphi_2) \\ y_1 &= r_1 \times \sin(\varphi_1) \\ y_2 &= r_2 \times \sin(\varphi_2) \end{aligned}, \tag{8}$$

where r_1 and r_2 are the radii of the outer and inner circular scans on retina respectively, and φ_1 and φ_2 are the azimuthal angles of the circular scans. The z coordinates were measured directly from the B-scan OCT images. Considering the retina is thin (~200μm) compared to the eyeball diameter (h =6 mm for rats), the coordinates of E' and S' can be expressed as

$$\begin{aligned} x_1' &= h \times \cos(\varphi_1) \\ x_2' &= h \times \cos(\varphi_2) \\ y_1' &= h \times \sin(\varphi_1) \\ y_2' &= h \times \sin(\varphi_2) \end{aligned}. \tag{9}$$

Experimentally, we unfolded the circular B-scan images from φ = 0 to 360 degree horizontally (supplementary Fig. S3c). The vertical axis z is the depth, where the low boundary of B-scan image was set as $z=0$. We manually segmented the vessels out from the outer and inner scanning circular B-scan images. Then the z coordinates as well as φ_1 and φ_2 could be measured. r_1 and r_2 can be calculated by

$$r_1 = h \cdot \tan(\phi_1),\ r_2 = h \cdot \tan(\phi_2) \tag{10}$$

The scanning angles ϕ_1 and ϕ_2 were set as 4 degree and 6 degree by the galvanometer mirrors, respectively. Given all the coordinates, the Doppler angle θ could be calculated according to Equ. 7.

3) **Blood vessel diameter calculation**. We directly measured the vessel height H axially from amplitude B-scan image. Note that OCT displays the optical path length delay between the sample and the reference. To obtain the physical height H, the optical path length needs to be scaled by $1/n$. n = 1.38 is the mean refractive index. The diameter of the blood vessel Dia was

$$Dia = H \times \sin(\theta)\ . \tag{11}$$

4) Phase wrap correction.

Because of the parabolic flow pattern, the blood velocity is low enough at the vessel wall to prevent phase-wrapping [5]. The flow direction can be determined by the phase value closed to the vessel wall. With the known blood flow direction, assume the actual phase $\Delta\phi < 0$, then after phase wrapping correction, we have

$$\Delta\phi = \begin{cases} \Delta\phi, \Delta\phi < 0 \\ \Delta\phi - 2\cdot\pi, \Delta\phi > 0 \end{cases}. \quad (12)$$

For the actual phase that is $\Delta\phi > 0$, the phase wrapping correction then can be corrected as

$$\Delta\phi = \begin{cases} \Delta\phi, \Delta\phi > 0 \\ \Delta\phi + 2\cdot\pi, \Delta\phi < 0 \end{cases}. \quad (13)$$

Microvasculature visualization. We obtained the volumetric data set and the surface topography from previous steps. We segmented a slab from the 3D volumetric dataset (from 150 to 200 μm away from the imaged retinal surface), and created a 2D mean intensity projection map from the slab. Then, we performed morphological closing with a 3 pixel radial disk pattern to obtain the inhomogeneous intensity background. At the end, we normalized the 2D mean intensity projection map by this background to enhance the contrast from the microvasculature.

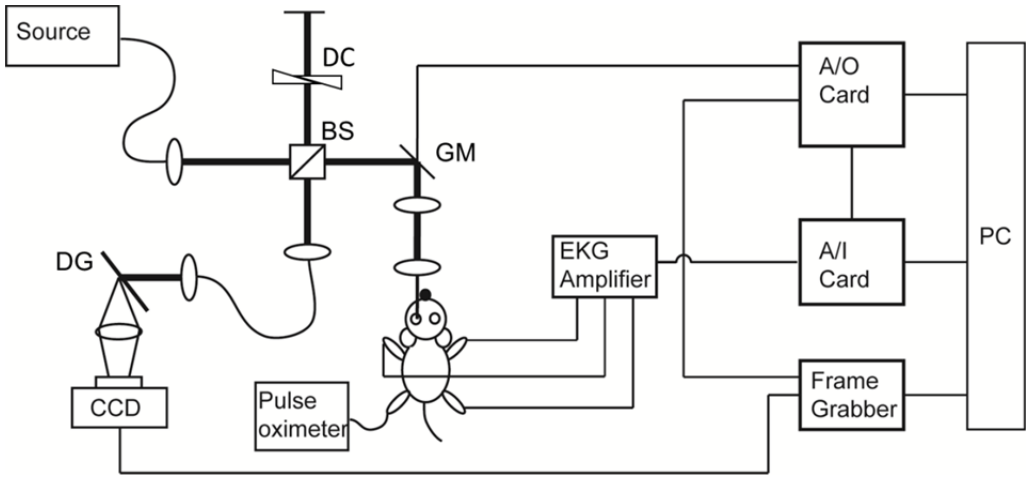

Figure S1. Schematic of the vis-OCT experimental system. The vis-OCT system used a supercontinuum laser source. The source is capable of providing broadband laser illumination from 500 nm to 620 nm. The output laser was collimated and split by a 50/50 cube beam splitter (BS) into the reference arm and sample arm. The reference arm is composed of a series of glass plates for dispersion control (DC), and a mirror to reflect the beam. The sample arm is composed of a two dimensional scanning galvanometer mirror (GM) to steer the beam direction, and a telescope lens system to relay the laser beam from GM to the rat eye pupil plane. The reflected beam from the sample and reference arm is recombined at BS and directed to a homemade spectrometer. The spectrometer is composed of a collimated lens, a diffraction grating (DG), an objective lens, and a line scanning camera (sprint2k140, Basler,). The EKG signals from rats were amplified by a three-lead EKG amplifier, and digitized by an analog input (A/I) digitizer card (PCI6251, National Instrument) at 12.5 Mega Sample/s. A clinically approved pulse oximeter was attached to the rat rear foot to monitor the arterial spO2 and heart rate. An analog output (A/O) card (PCI6731, National Instrument) was used to provide the synchronization signal to GM, EKG amplifier, and the CCD frame grabber.

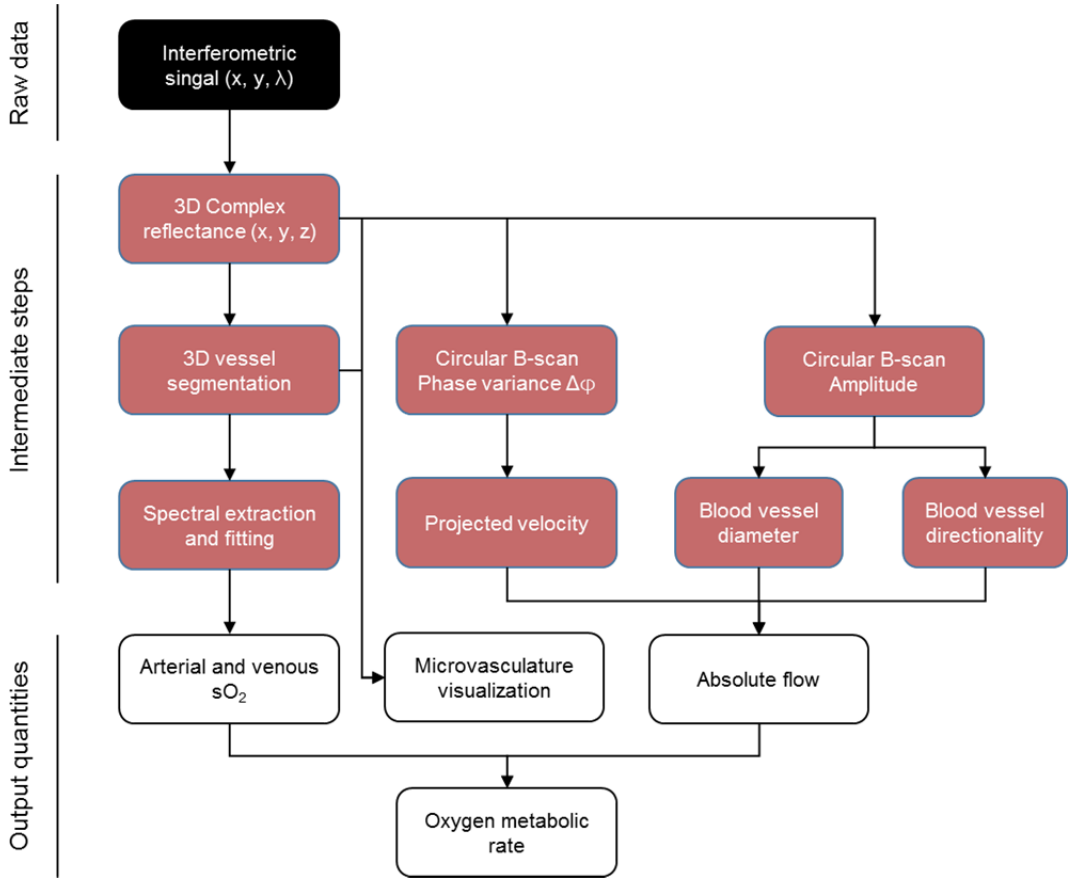

Figure S2. Flow chart of data processing to obtain retinal oxygen metabolic rate ($rMRO_2$). The raw interferometric spectral data was acquired by the line-scan CCD in the home-made spectrometer. The subsequent data processing extracted the localized spectra from retinal blood vessels, and calculated the blood flow from the phase variance contrast between adjacent A-line scans.

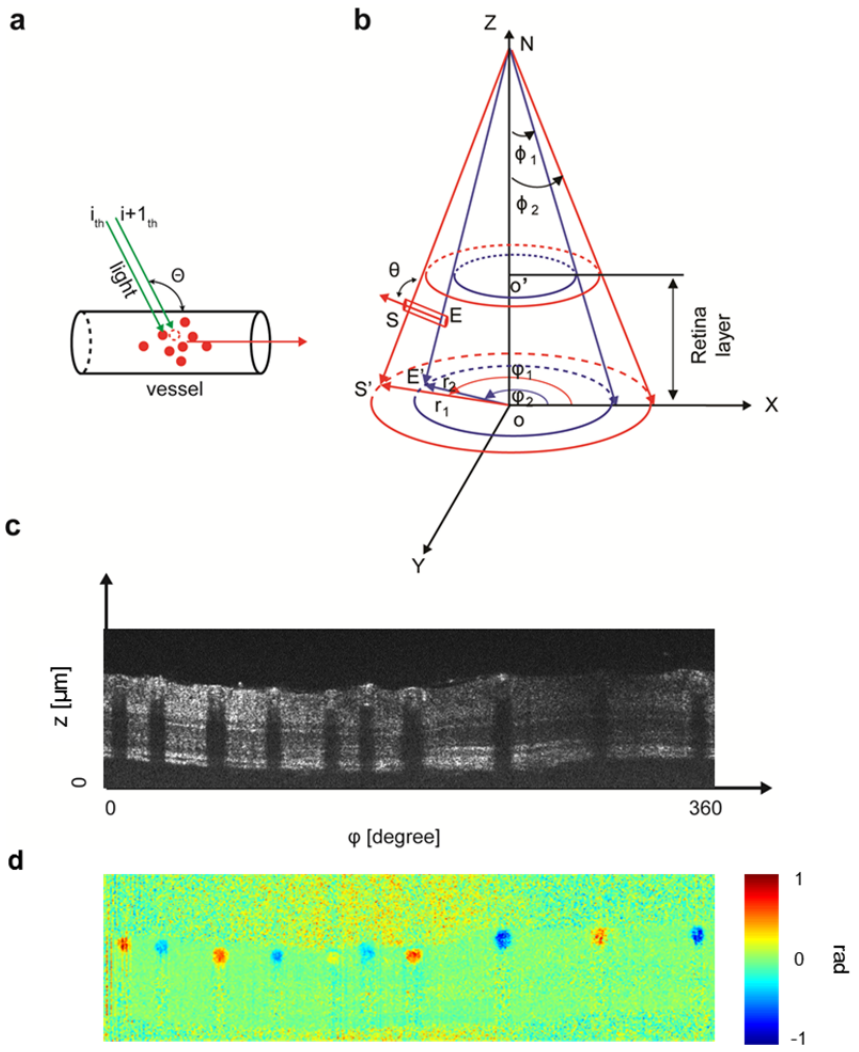

Figure S3. Demonstration of retinal blood flow measurement *in vivo*. (a) Diagram showing flow contrast by moving red blood cells. The phase shift of the complex reflectance signal from two adjacent A-lines is proportional to the flow velocity projected to the light beam. (b) The geometry for calculating Doppler angle by dual circle scanning pattern. The Doppler angle θ is between the blood vessel vector *SE* and the beam direction *NS'*. The detailed mathematical model is described in the following sections. (c-d) An example of an unfolded B-scan image from the inner circular scan and its corresponding phase shift B-scan image.

Supplementary table for heart rate measurements. Heart rates measured by pulse oximetry under different breathing oxygen content. P-values are calculated comparing to 21% O_2 group by two-tailed two-sample t-Test.

Subject	21% O_2	19% O_2	16% O_2	14% O_2	11% O_2	9% O_2
1	281	280	285	294	297	291
2	298	290	321	345	327	303
3	280	281	282	300	289	306
4	314	323	310	289	281	300
5	291	299	301	314	297	298
6	344	356	360	346	352	360
7	270	277	285	297	279	270
8	300	311	319	312	298	287
9	233	231	222	228	253	237
10	193	197	205	220	238	206
Mean	280.4	284.5	289	294.5	291.1	285.8
SEM	13.3	14.2	14.6	13.3	10.3	13.2
P-value	--	0.83	0.67	0.46	0.53	0.77

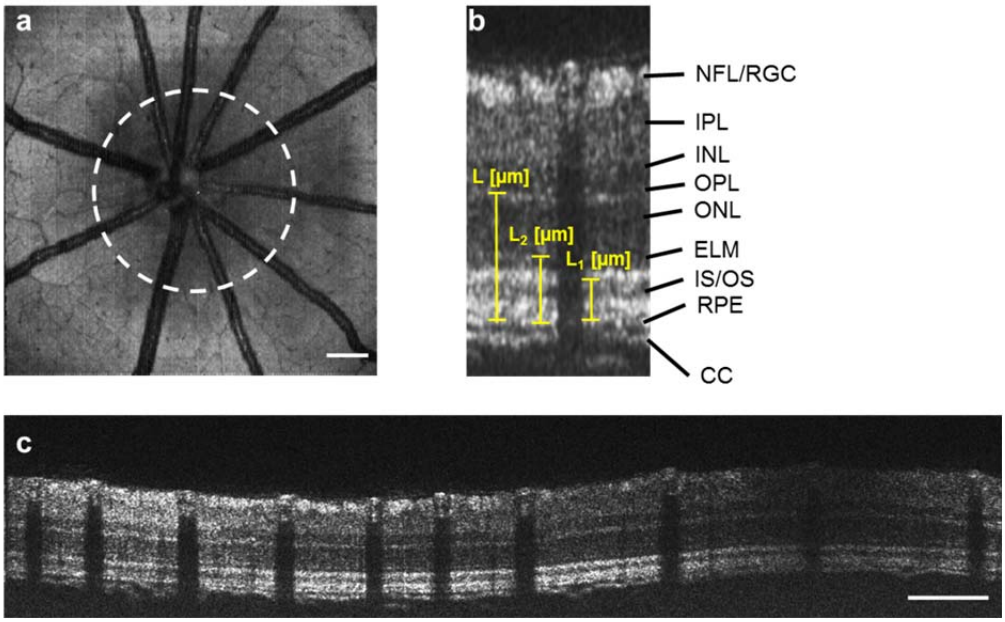

Figure S4. Vis-OCT images of rat retina. (a) A retinal fundus image by mean-intensity-projection along the depth direction. The white dashed-circle is the circular scanning trajectory for the B-scan image shown in panel c. Bar: 200 μm. (b) Magnified B-scan cross sectional image. Different retinal layers are labeled on the right side. L_1 and L_2 [μm] are the distance from the choroid to the beginning of the inner segment (IS) of the photoreceptor and distance from choroid to the outer nuclear layer (ONL), respectively; L [μm] is the thickness of the outer retina. NFL: nerve fiber layer; RGC: retinal ganglion cell; IPL: inner plexiform layer; INL: inner nuclear layer; OPL: outer plexiform layer; ONL: outer nuclear layer; ELM: external limiting membrane; IS/OS: inner outer segment junction of photoreceptors; RPE: retinal pigment epithelium; CC: choroiocapillaris. Bar: 100 μm. (c) B-scan image acquired from the circular scanning around the optic disk. Bar: 200 μm.

Supplementary methods for flow verification

We conducted a phantom experiment to verify our flow measurements. The telescope in the sample arm was replaced by a telecentric objective lens (Supplementary Fig. S5a). The phantom is consisted of a capillary tube (Paradigmoptics, CTPS125-250; Inner diameter: 125 μm) connected to a syringe pump (A-99, Razel). A 1% intralipid solution was pumped though the capillary tube, and the flow rate was controlled by the syringe pump. The measured flow rates were calibrated with the settings on the syringe pump.

Because laser beam was focusing nearly perpendicularly to our sample, we defined the Cartesian coordinate system with the *z* axis against the beam direction (supplementary Fig. S5a). The Doppler angle is equal to the angle between the flow vector direction and the z axis. Supplementary Fig. S5b shows one example of the 3D rendering of a capillary tube. The three dimensional coordinates can be directly read from the 3D images at any given point A(x_1, y_1, z_1), and B(x_2, y_2, z_2) in the tube. The cosine of the Doppler angle is calculated as

$$\cos(\theta) = (z_2 - z_1)/\sqrt{(x_2 - x_1)^2 + (y_2 - y_1)^2 + (z_2 - z_1)^2}\,. \tag{14}$$

We tested various flow rates within the normal physiological range controlled by a syringe pump (A-99, Razel). Supplementary Fig. S5c and S5d are the amplitude and phase of the B-scan image. We measured the inner tube diameter to be 129.5 ± 2.6 μm from the amplitude B-scan image, and the Doppler angle θ to be 82 ± 1 degree, which agreed well with the preset Doppler angle of 81 degree. We tested the flow rate ranging from 0.4 μl/minute to 9 μl/minute; as shown in Supplementary Fig. S5e. The measured results were consistent with the preset flow rate.

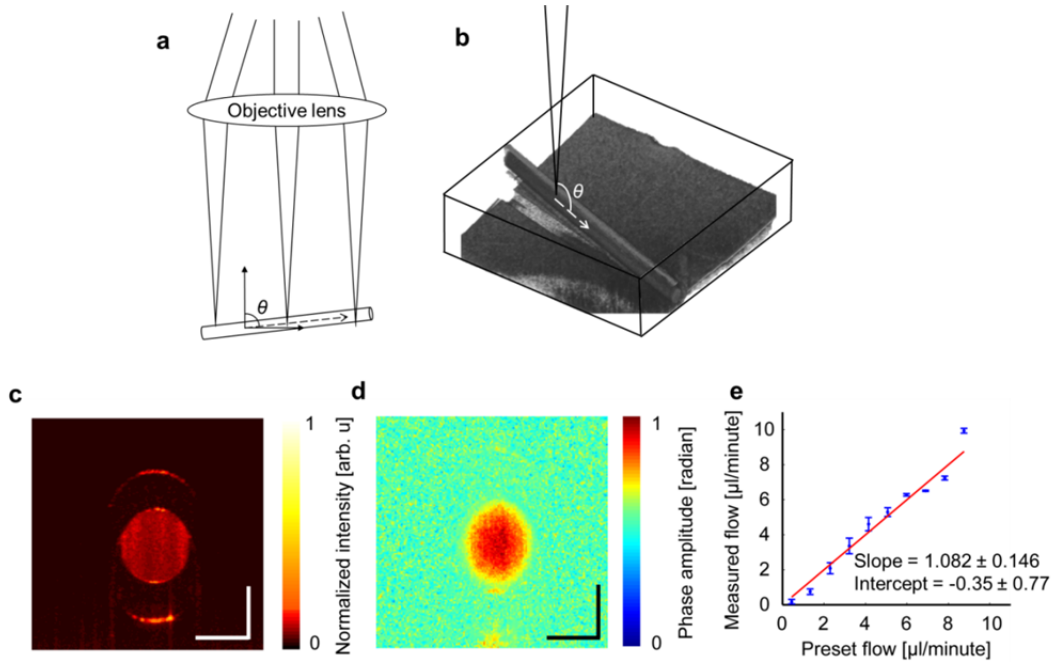

Figure S5. Verification of vis-OCT flow measurment in a flow phantom. (a) Schematic of the telecentric optical scanning in the sample arm. (b) 3D rendering of a capillary tube with respect to the beam. (c) Amplitude and (d) phase OCT B-scan image from the capillary tube; Bar: 100 µm. (e) Comparison between the measured flow results and the preset flow rate. The result of the linear regression is shown.

Supplementary methods for *in vitro* sO_2 verification

We used bovine whole blood with known sO_2 to calibrate our sO_2 measurements. We prepared an oxygenated blood stock by exposing the blood to air for an hour, and a deoxygenated blood stock by a surface flow of nitrogen for an hour (supplementary Fig. S6a). The blood stocks were contained in flasks and stirred gently on a rocker. Next, a layer of mineral oil was poured on top of the whole blood to prevent the air exposure and preserve the oxygenation. To determine the sO_2 from the blood stock, we sampled the blood and tested with a blood analyzer (Rapidlab, Siemens). The O_2 tension, CO_2 tension, pH value were measured and adjusted under the room temperature (22 degree C) (supplementary Fig. S6b). We then calculated the sO_2 from the Kelman's equation [6]. The sO_2 for the oxygenated and deoxygenated blood stock were calculated as 98.5% and 39.9%. Next, we mixed two blood stocks by different volumetric ratios to make a series of blood samples with gradually changing oxygenation levels. The sO_2 from each blood sample is then by definition: $sO_2=0.985x+0.399(1-x)$, where x is the relative content of oxygenated blood stock. Supplementary Fig. S6a shows the blood samples that we prepared. Each blood sample was sealed by a layer of mineral oil to preserve the oxygenation.

We then filled a capillary tube (Paradigmoptics, CTPS125-250; Inner diameter: 125 μm) with the sample blood by a syringe pump, and imaged with vis-OCT. The spectra were taken from the bottom inner surface of the tube, and the same algorithm was implemented to calculate sO_2. The calibration results are shown in Supplementary Fig. S6c.

a

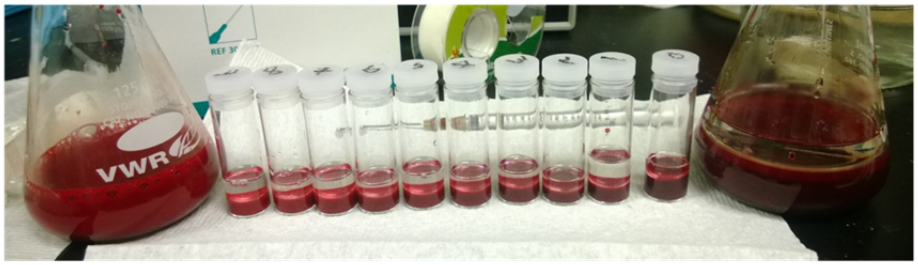

b Bovine blood parameter *in vitro*

	Oxy	Deoxy
PO_2(mmHg)	105.3	17.5
PCO_2(mmHg)	5	5
PH	7.320	7.570
Temperature(c)	37	37
sO_2 (percent)	98.5	39.9

c

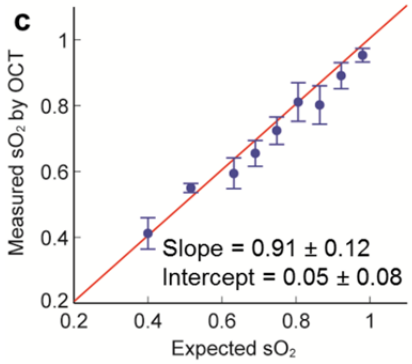

Figure S6. Verification of vis-OCT sO_2 measurement *in vitro*. (a) Photograph of different ratios of oxygenated and deoxygenated bovine whole blood samples. The left most flask was oxygenated blood with a bright red color, and the right most flask was deoxygenated blood with a dark red color. The oxygenation of the blood in the small bottles decreased from ~98% to ~40% from left to right (by mixing fully oxygenated and fully deoxygenated blood at different volumetric ratios), as the color gradually became darker. (b) Representative blood parameters measured by blood gas analyzer (Siemens, Rapidlab) from oxygenated (Oxy) and deoxygenated (Deoxy) blood stock. (c) Comparison between the expected and measured sO_2 values. The result of the linear regression was listed. n=3 measurements.

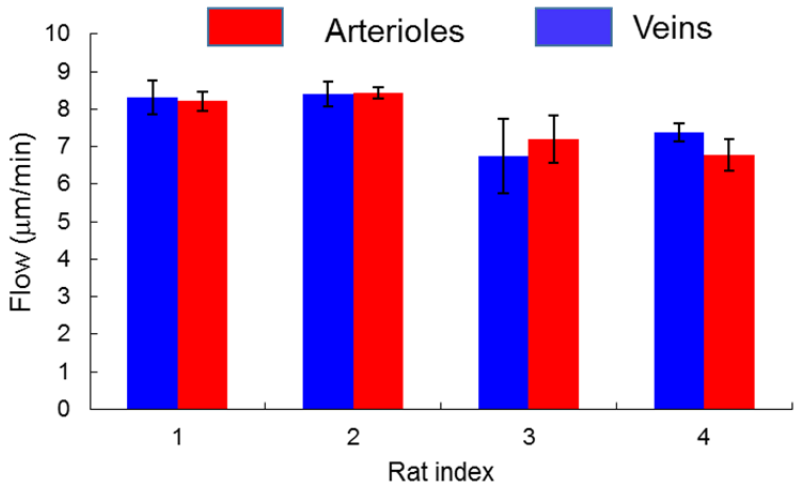

Figure S7. Retinal flow measurements from the major retinal arterioles and veins (n = 4 rats). The mean values of 8 repeated measurements from arterioles and veins. Error bar is the standard errors of the 8 measurements. The averaged standard error characterized the measurement precision. None of the arteriovenous flow pairs reached statistically significance using two student T-tests for comparison (P=0.57, 0.74, 0.67, 0.24, respectively).

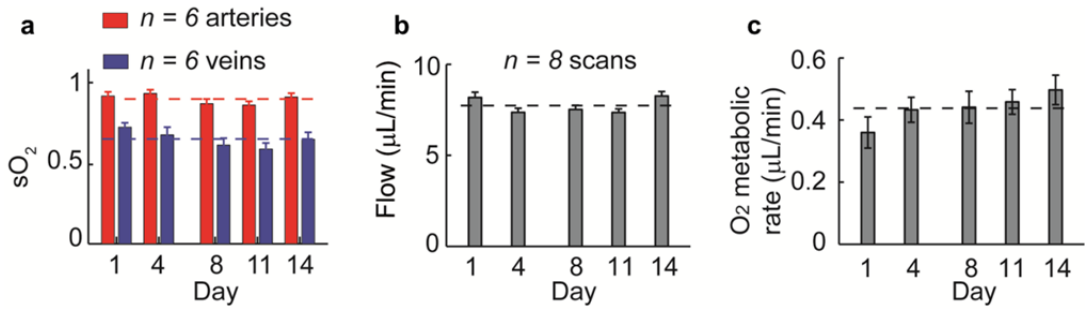

Figure S8. Vis-OCT longitudinal stability studies of (a) sO_2, (b) flow, and (c) $rMRO_2$ *in vivo*. Five measurements were taken on same subjects over two weeks. Dashed line marks the mean values of the five measurements.

Supplementary methods for oxygen tension profile in outer retina

The outer retina was modeled as a three layer semi-infinite slab. From the choroidal to inner retinal side, the three layers are photoreceptor outer segments (Layer 1), photoreceptor inner segments (Layer 2), and the outer nuclear layer (Layer 3). We used the second order Fick's law to model this one-dimensional oxygen tension profile [7],

$$Q = Dk\frac{d^2P}{dx^2}, \tag{15}$$

where Q is oxygen consumption normalized by the tissue weight [ml ·min^{-1}·100g^{-1}], D is diffusivity of oxygen [1.97x10^{-5} cm^2/s], k is solubility of oxygen [2.4ml O_2/ (ml retina·mmHg)], P is PO_2 [mmHg], and x is the distance from the choroid. The oxygen consumption is confined to Layer 2. Thus, Q_1 and Q_3 were considered negligible and set to zero in Layer 1 and 3. By solving Equ. 15, we obtained PO_2 profile in each layer,

$$\begin{aligned} &P_1(x) = \alpha_1 x + \beta_1 \quad 0 < x < L_1 \quad Layer\ 1 \\ &P_2(x) = \frac{Q_2}{2Dk}x^2 + \alpha_2 x + \beta_2 \quad L_1 < x < L_2 \quad Layer\ 2 \\ &P_3(x) = \alpha_3 x + \beta_3 \quad L_2 < x < L \quad Layer\ 3 \end{aligned} \tag{16}$$

where α and β are constants that can be determined from the boundaries conditions (matching PO_2 and O_2 flux at the boundaries between layers). Thus,

$$\begin{aligned} \beta_1 &= P_C, \\ \beta_2 &= \frac{Q_2}{2Dk}L_1^2 + P_C, \\ \beta_3 &= \frac{Q_2}{2Dk}L_2^2 + \beta_2, \\ \alpha_3 &= (P_L - \beta_3)/L, \\ \alpha_2 &= -L_2\frac{Q_2}{Dk} + \alpha_3, \\ \alpha_1 &= L_1\frac{Q_2}{Dk} + \alpha_2. \end{aligned} \tag{17}$$

The parameters used in the simulation are listed below, and were obtained for rat retina by Ref. [7]. The simulated PO_2 profile is illustrated in supplementary Fig. S9.

Table 1 Characteristics of oxygen distribution and consumption in the simulation

Characteristics of oxygen distribution and consumption	
L1 (μm)	25
L2 (μm)	46
L (μm)	85
PO_2 at L, P_L (mmHg)	28.8 [8]
Q_{av} (ml ·min^{-1}·100g^{-1})	1.8
$Q_2=Q_{av}L/(L_2-L_1)$	7.3
Outer retina weight (mg)	6

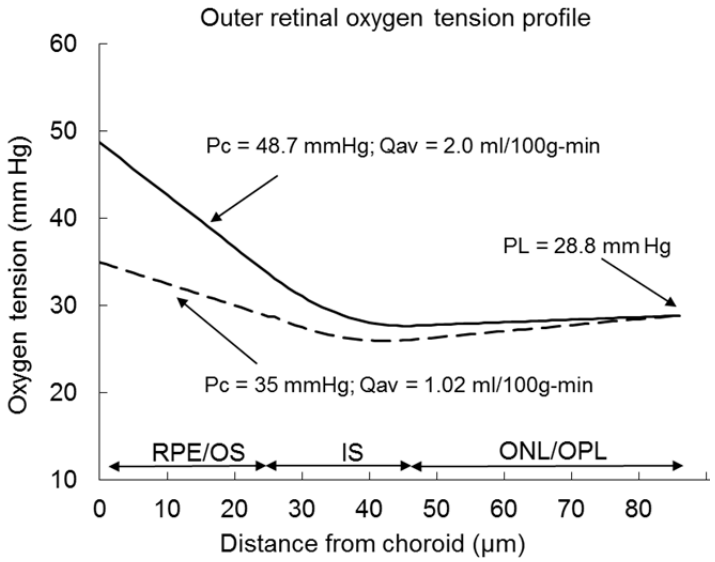

Figure S9. Simulated oxygen tension (PO_2) profiles as a function of distance from choroid. The choriocapillaris is located at 0 μm along the horizontal axis, and the interface between outer retina and inner retina is located at 85 μm. Retinal pigmented epithelium (RPE)/outer segment of photoreceptor (OS) layer (Layer 1), and the outer nuclear layer (ONL)/outer plexiform layer (OPL) (Layer 3) has the linear profile of PO_2; while inner segment of photoreceptor (OS) (Layer 2) has a quadratic PO_2 profile. Solid line is the PO_2 profile under normal air breathing, and the dashed line is under systemic hypoxia at P_aO_2 =72 mmHg. The choroidal oxygen tension (Pc) is proportional to the systemic P_aO_2. The oxygen tension at the interface between outer and inner retina (PL) is considered to be the same due to the autoregulation of the retinal circulation. Model and parameters for light adapted rat retina are based on Ref. [7].

Supplementary laser safety evaluation for vis-OCT

We calculated the laser safety requirement for vis-OCT according to the American National Standard for safe use of lasers (ANSI 2007). We measured the angular subtense α = 7.3 mrad for our illumination. As a result, the vis-OCT illumination source is an extended light source. And we have $\alpha_{min}<\alpha<\alpha_{max}$, where α_{min} (1.5 mrad) and α_{max} (100 mrad) are the minimal and maximal subtense angles, respectively, for wavelengths between 0.4 and 1.4 μm defined in Ref. [9]. According to Table 6 of Ref. [9], the correction factors and C_E is α/α_{min}= 4.87. The supercontinuum laser used in our vis-OCT system is a high repetition rate pulsed laser with pulse rate of 80MHz. The pulse width varies from 20-40 ps depending on the wavelength. We took 30ps pulse width at 580nm for any necessary calculation. Because of the pulsed laser nature, we followed the standard described in section 8.2.3, page 64 in ANSI standard.

Rule 1: Single pulse limit (MPE_{SP}). This rule requires that "the exposure from any single pulse in a train of pulses shall not exceed the MPE for a single pulse of that pulse duration". Because the repetition rate is very high (80MHz) and pulses are considered to have equal energy, this rule will be automatic satisfied if the entire pulse train is under the safe exposure threshold, which will be calculated and described below.

Rule 2: Average power limit for thermal hazard (MPE_{GROUP}). This means that "the total radiant exposure of all pulses within any part of the train shall not exceed the MPE for the exposure time t." Our scanning protocol covers a retina area around 7.8 mm^2 (scanning angle = 25 degree, rat eye diameter = 6mm), and took 2.6s to finish. The FWHM diameter of the focal spots were estimated as 20μm, giving the focal area of $3.14 \times 10^{-4} mm^2$. The averaged exposure time is $t = 2.6 \times \frac{3.14\times10^{-4}}{7.8} s = 1.04 \times 10^{-4} s$. The photochemical hazard limit at visible wavelength 0.4-0.7μm for point source ocular exposure is $5C_E \times 10^{-7} J \cdot cm^{-2}$. The permitted power density of the laser is then $24.35 mW \cdot cm^{-2}$. Given the diameter of the dilated rat pupil diameter of 3 mm, the averaged permitted power from laser is 1.72mW.

Rule 3: Multiple pulse limit for thermal hazard (MPE_{MP}). "Rule 3 applies only to MPEs for thermal injury, where all pulses delivered in less than t_{min} are treated as a single pulse. For individual pulses or groups of pulses, either delivered within a time frame less than t_{min}, or when the inter-pulse spacing between pulses or pulse groups is less than t_{min}, these pulse structures are treated as a single pulse in applying this rule." The repetition rate of the source is 80MHz, giving the inter-pulse spacing 12.5ns. For a visible light source, t_{min} is equal to 18μs. Thus, we treated the pulse train during our exposure as one single pulse, or a continuous source. In this case, the MPE is the same as the one governed by Rule 2.

We measured the averaged power entering the pupil to be ~0.8mW by a power meter

(Newport, 1918-R), which is below the safety standard.

Reference:

1. N. Otsu, "A threshold selection method from gray-level histograms," IEEE Transactions on Systems, Man and Cybernetics **9**, 62-66 (1979).
2. J. Yi, Q. Wei, W. Liu, V. Backman, and H. F. Zhang, "Visible-light optical coherence tomography for retinal oximetry," Optics Letters **38**, 1796-1798 (2013).
3. Y. Wang, B. A. Bower, J. A. Izatt, O. Tan, and D. Huang, "In vivo total retinal blood flow measurement by Fourier domain Doppler optical coherence tomography," J. Biomed. Opt. **12**, 041215 (2007).
4. Y. Wang, B. A. Bower, J. A. Izatt, O. Tan, and D. Huang, "Retinal blood flow measurement by circumpapillary Fourier domain Doppler optical coherence tomography," J. Biomed. Opt. **13**, 064003 (2008).
5. A. S. G. Singh, C. Kolbitsch, T. Schmoll, and R. A. Leitgeb, "Stable absolute flow estimation with Doppler OCT based on virtual circumpapillary scans," Biomedical Optics Express **1**, 1047-1059 (2010).
6. G. R. Kelman, "Digital computer procedure for the conversion of PCO2, into blood CO2 content," Respiration Physiology **3**, 111-115 (1967).
7. J. C. M. Lau and R. A. Linsenmeier, "Oxygen consumption and distribution in the Long-Evans rat retina," Experimental Eye Research **102**, 50-58 (2012).
8. R. A. Linsenmeier and R. D. Braun, "Oxygen distribution and consumption in the cat retina during normoxia and hypoxemia," The Journal of General Physiology **99**, 177-197 (1992).
9. A. N. S. I. (ANSI), "American national standard for the safe use of lasers," Standard Z136.1-2007 (Laser Institute of America, Orlando, FL, 2007).